IEEE Robotics and Automation Letters (RA-L) paper, presented at ICRA 2024, Yokohama, Japan. Cite as RA-L paper.

Tetraflex: A Multigait Soft Robot for Object Transportation in Confined Environments

Peter Wharton[1,4*], Tsam Lung You[2,4*], George P. Jenkinson[3,4], Richard Suphapol Diteesawat[2,4], Nguyen Hao Le[2,4], Edith-Clare Hall[2,4], Martin Garrad[2,4], Andrew T. Conn[3,4] and Jonathan Rossiter[2,4]

***Abstract*—Unstructured environments call for versatile robots with adaptable morphology that can perform multiple goal-directed actions including locomotion in confined spaces, environmental mapping, object retrieval and object manipulation. In response to these challenges, we present the Polyflex design concept for fabrication of modular, soft truss robots and demonstrate its varied capabilities in a tetrahedral robot (Tetraflex). Tetraflex is composed of six pneumatically actuated bellows joined at four points by rigid nodes. By extending or contracting the bellows, Tetraflex is capable of large size and shape change, and rolling, crawling and bounding gaits. Furthermore, Tetraflex is able to roll onto and engulf objects then subsequently transport them with the crawling gait. The rolling gait discretises Tetraflex's locomotion into predictable steps on a triangular grid, simplifying odometry and allowing the use of path planning to attain a desired position. The size of rolling step can be changed at any time by dynamically varying the size of the robot. The crawling and bounding gaits enable Tetraflex to move in smaller incremental steps or through narrow passages (80 mm wide). The maximum speed was attained with a bounding locomotion gait at 19.6 mm/s (0.15 body lengths per second, or BL/s). Rolling locomotion attained between 15.6 and 19.4 mm/s (0.12-0.15 BL/s), and crawling 7.8 mm/s (0.06 BL/s). The rolling gait was the most accurate gait, achieving 2.3% linear deviation. The flexibility and versatility of Tetraflex in morphology, locomotion and object transportation demonstrates its suitability for deployment in a wide range of environments and for applications including surveying, search and rescue, and remote sample collection.**

***Index Terms*—Soft Robot Applications, Soft Robot Materials and Design, Search and Rescue Robots**

I. Introduction

Manuscript received: January, 31st, 2023; Revised May, 9th, 2023; Accepted June, 6th, 2023.

This paper was recommended for publication by Editor Yong-Lae Park upon evaluation of the Associate Editor and Reviewers' comments.

This work was supported by the following grants: PW is supported by Engineering and Physical Sciences Research Council (EPSRC) grant EP/S021795/1 (Centre for Doctoral Training in Future Autonomous and Robotic Systems—FARSCOPE). TLY is supported by the Croucher Foundation through the Croucher Scholarships for Doctoral Study. GPJ is supported by EPSRC grant EP/R513179/1. RSD is supported by EPSRC grant EP/S026096/1. ECH is supported by EPSRC grant EP/T517872/1. JR is supported by EPSRC grants EP/V062158/1, EP/S021795/1, EP/R02961X/1, EP/V026518/1, and EP/T020792/1, and the Royal Academy of Engineering through the Chair in Emerging Technologies scheme, CiET1718/22. AC is supported by EPSRC grants EP/R02961X/1 and EP/T020792/1.

*These authors contributed equally

[1]The authors are with the Department of Aerospace Engineering [2] Department of Engineering Mathematics, [3] Department of Mechanical Engineering and [4] Bristol Robotics Laboratory, University of Bristol, Bristol, BS8 1TR, UK

Correspondence: peter.wharton@bristol.ac.uk

Digital Object Identifier (DOI): see top of this page.

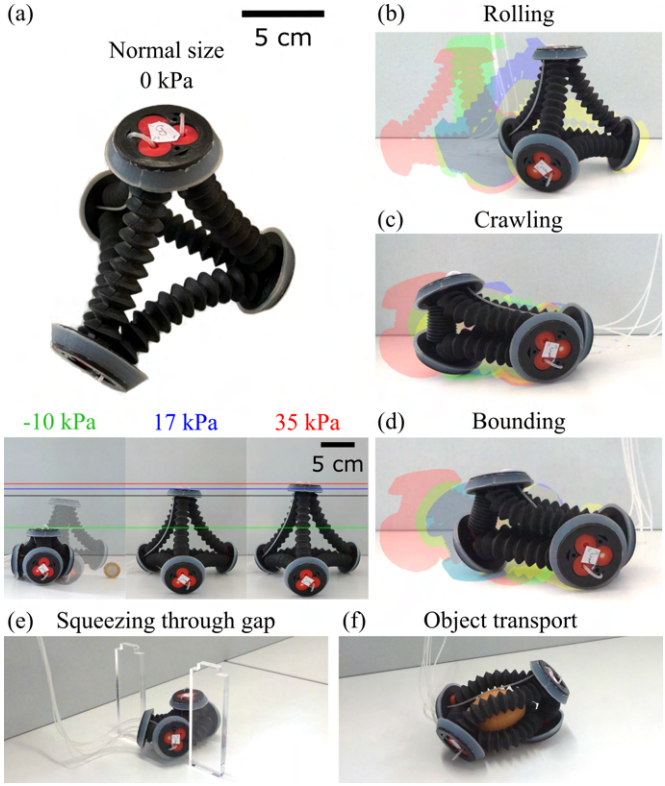

Fig. 1: Tetraflex is composed of six bellows, joined by four end caps. (a) Shape and size change by varying bellows pressure (lines indicate robot height; transparent robot is the natural size at atm). (b-d) Controlled bellow inflation and deflation for (b) rolling, (c) crawling, and (d) bounding locomotion (colors illustrate locomotion progress). (e) Crawling locomotion to pass through narrow gap. (f) Transporting an engulfed object.

UNSTRUCTURED environments require adaptable robots to facilitate exploration and to carry out a multitude of tasks such as manipulation, structural stabilisation, and object transportation. For environments with low resource availability such as space exploration, design methodologies have emerged which exploit large shape change and a modular architecture, aiming to create robots capable of achieving many tasks without requiring redesign or modification.

One such design methodology is Tensegrity [1], which uses rigid interlinked objects joined by tensile cables. The resultant structure is compliant and can perform large shape change through active control of cable tension [2], [3]. Another

IEEE Robotics and Automation Letters (RA-L) paper, presented at ICRA 2024, Yokohama, Japan. Cite as RA-L paper.

IEEE Robotics and Automation Letters (RA-L) paper, presented at ICRA 2024, Yokohama, Japan. Cite as RA-L paper.

approach utilises a truss architecture, composed of a set of struts and connecting nodes in a mesh [4], [5]. This approach has the potential for mobility in challenging environments, object engulfment and subsequent transport. Truss robots have been investigated both in modelling and simulation [6]–[8] and physically [9]–[11]. To date there has been limited investigation into soft truss architectures, with the notable exception being Usevitch et al. which combined soft materials with truss architectures to make a robot that can locomote and support and lift objects. However, the size and shape change capability of the robot is limited by an isoperimetric constraint [12]. Previous robots using adjustable soft trusses have been limited to 2D profiles in triangular and circular configurations [13]–[15].

Some soft robots have been created for the task of transporting objects: these include an ant-inspired robot which can grasp objects and locomote with them [16], and some examples of small scale robots, actuated via magnetic SMA heating [17] or electromagnetically [18] which can carry a load but can't grasp objects or engulf them for protection.

Here we present the Polyflex design concept for creation of modular soft truss robots. Polyflex utilises rubber bellows for struts which are sealed and connected to pneumatic inputs. By modulating the input pressure, the length of the bellow strut can be changed, thus changing the shape and size of the Polyflex assembly. This is similar to the models proposed in [19]–[21], though in the case of Polyflex variable length struts are achieved using soft actuators. Additionally, due to the modular and easy to assemble architecture, various robot configurations can be exploited without needing additional hardware or major reconstruction. The use of primarily soft materials also enables Polyflex robots to interact with fragile objects or biological organisms safely, and adapt to unknown and unstructured environments [22], [23]. Large size changes are possible with Polyflex architectures, allowing passage through enclosed spaces and easier storage. In this work, we demonstrate the Polyflex concept with a robot composed of 6 struts arranged in a tetrahedral configuration, henceforth referred to as Tetraflex (Fig. 1). Other configurations are possible such as a cube structure which could be used for supporting horizontal platforms or inching within a tube. Higher order Polyflex implementations provide increasingly flexible shape changing ability, at the cost of increased control and actuation requirements.

A number of Tetrahedral robots have been explored previously, including rigid structures using linear actuators as struts [24], and robots using revolute mid-strut actuators [25]–[27]. Soft tetrahedral robots can have struts that bend and twist to produce complex shape change [28], but are constrained in size. Tian et al. developed a soft tetrahedral robot fixed at the base to facilitate wrist rehabilitation exercises [29], similarly novel pneumatic actuators arranged in a tetrahedral configuration were used for manipulation of a 200 g mass [30]. Wang et al. present a robot using a single central node and four radially branching soft legs, where each leg can bend to achieve rolling and crawling locomotion [31]. In contrast, the proposed Tetraflex not only achieves effective locomotion, but can also dynamically change its size and capture and transport objects. Tetraflex's morphing abilities allow it to move through a narrow gate, roll onto an object, and crawl with the object still engulfed within the robot structure (Fig. 1).

In this paper, we present the Polyflex design and the implementation in the Tetraflex robot in section II. Experimental results are shown in section III, including consistency and speed results for three gaits and a demonstration of Tetraflex's object transport abilities. The work concludes with a discussion of results and conclusions in section IV.

II. Design and Concept

We define Polyflex configuration through the set $V = \{v_1, ..., v_j\}$ of j nodes, and the set $S = \{s_1, ..., s_i\}$ of i strut connections, where each s_x designates the pair of nodes that are connected by a strut. In order to demonstrate the capabilities of the Polyflex architecture, we develop a tetrahedral Polyflex robot (Tetraflex), composed of six bellow struts connected by four end cap nodes. Tetraflex is defined as $V = \{a, b, c, d\}$ and $S = \{\overline{ab}, \overline{ac}, \overline{ad}, \overline{bc}, \overline{bd}, \overline{cd}\}$. In this case, we also define the faces that oppose the nodes V as $F = \{A, B, C, D\}$. Tetraflex is capable of locomotion through small gaps, precise rolling locomotion, object grasping/engulfment and object transport.

A. Design and Fabrication

The key elements of Tetraflex are the six linearly actuating soft elastomer struts and the nodes connecting the actuators. For the struts we developed pneumatic actuators composed of rubber bellows with an external diameter of 20 mm and a resting length of 106.3±1.6 mm (CABCOV, Car Builder Solutions, UK). They are sealed by inserting plugs on both ends of the bellow, with one plug having an integrated silicone tube to connect to the pneumatic supply. Six of such actuators were then connected together by end caps in a tetrahedral configuration (Fig. 1a). The plugs and the end caps were 3D printed polylactic acid (PLA). Each is tapered at 60°, and a thin (2 mm) silicone (Ecoflex 00-30, Smooth-On, Inc., Macungie, PA, USA) covering is attached to the end cap to increase friction and reduce sliding during rolling locomotion. The outer ring of the PLA end cap is left uncoated, causing an angle dependent friction asymmetry which is utilised in the crawling locomotion (Fig. 2a).

In order to achieve bellow actuation, we connect Tetraflex to an electro-pneumatic system (Fig. 2c). Each of the six bellows is connected to a 2/2 solenoid valve (CJAV08-2B05A1, Conjoin, China) and a 3/2 solenoid valve (S070C-RAG-32, SMC, Japan) in sequence, with an additional two pairs of 2/2 and 3/2 valves which are used to modulate the pressure sources. Each bellow can exist in one of four different pressures (Fig. 2c): atmospheric pressure (atm) used for venting; high positive pressure P_{high} used for active bellow inflation; negative pressure from the vacuum pump P_{-ve}; and low positive pressure P_{low} used to control the default size of Tetraflex. Both positive pressures are set by pressure regulators (SMC AR20-F02H-1-B, SMC, Japan), which are connected to a compressor (P100/24 AL, Werther International S.p.A., Germany). A 12V pump (ROB-10398, SparkFun, US) is used to generate the

IEEE Robotics and Automation Letters (RA-L) paper, presented at ICRA 2024, Yokohama, Japan. Cite as RA-L paper.

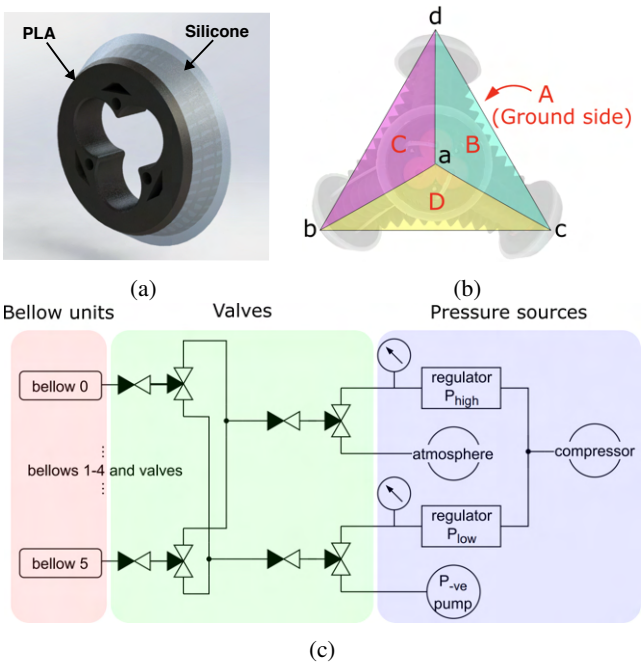

Fig. 2: (a) Detail of end cap. (b) Top view of Tetraflex with annotations, showing nodes and faces. (c) Schematic diagram of the pneumatic circuit.

vacuum (P_{-ve}) pressure. The endcaps of Tetraflex align the bellow ends in parallel which results in a slight inward bend in the bellows (see Fig. 1a). Due to the compliant nature of the bellows, there is a tendency for them to straighten during inflation, generating torque on the end caps and their consequential realignment to a new equilibrium position. The compliance of the bellows, however, means that the angle at which they are fixed to the end caps is less important than for rigid struts, and complex bending of the bellows (as seen in Fig. 1f where an egg is held) is possible.

B. Locomotion strategy

Tetraflex locomotes by cyclic inflation and deflation of the bellows. Varying the sequence and combination of bellow inflation and deflation enables Tetraflex to perform rolling, crawling, and bounding gaits. The rolling locomotion takes discrete steps for more predictable positioning, whilst the crawling and bounding gates take smaller steps and are capable of passing through narrow gaps. We describe the various gaits by reference to labelled example in Fig. 2b, with node set $V = \{a,b,c,d\}$, strut set $S = \{\overline{ab},\overline{ac},\overline{ad},\overline{bd},\overline{cd},\overline{bc}\}$ and face set $F = \{A,B,C,D\}$.

1) Rolling: By modulating bellow sizes, an instability can be created which causes the Tetraflex structure to roll over its centre of mass (COM) from the current ground (bottom) face to any other face. In doing so, the robot takes a predictable step which is dependent on its default bellow size. For example, when rolling from ground face A to face B, Tetraflex rolls over a 'pivot bellow' $\overline{cd}$ (Fig. 3a). To achieve this roll, the other two bellows which comprise the base triangle, designated as 'leg bellows' (bellows $\overline{bd}$ and $\overline{bc}$ in this case), contract, making the base area smaller and reducing stability. In order to trigger the roll, inflation of the 'backbone bellow' (bellow $\overline{ab}$ in this case) takes place, causing a differential bending of the structure and moving the COM outward beyond the base of support and causing Tetraflex to roll. After completing a roll, Tetraflex returns to its original shape in preparation for the next motion. Fig. 5a shows a sequence of images of Tetraflex undergoing a single roll. All bellows which hold constant pressure during locomotion are defined as structural bellows. Structural bellows in rolling maintain the 'default' pressure, which determines the 'default size' of Tetraflex. A larger default size, formed by higher default pressure, results in larger steps taken.

As the net motion of a Tetraflex roll is linear, we project the masses of the Tetraflex onto the 2D plane in which it moves in order to model the rolling motion. Here, we model all bellows as straight lines of variable length with mass m situated at the centre of each bellow. A limitation of the model is that bellow struts bend during operation. Due to the symmetry of Tetraflex, it can be modelled as a simple triangle connecting the in-plane $\overline{ab}$ bellow to the centre of the perpendicular $\overline{cd}$ bellow at the

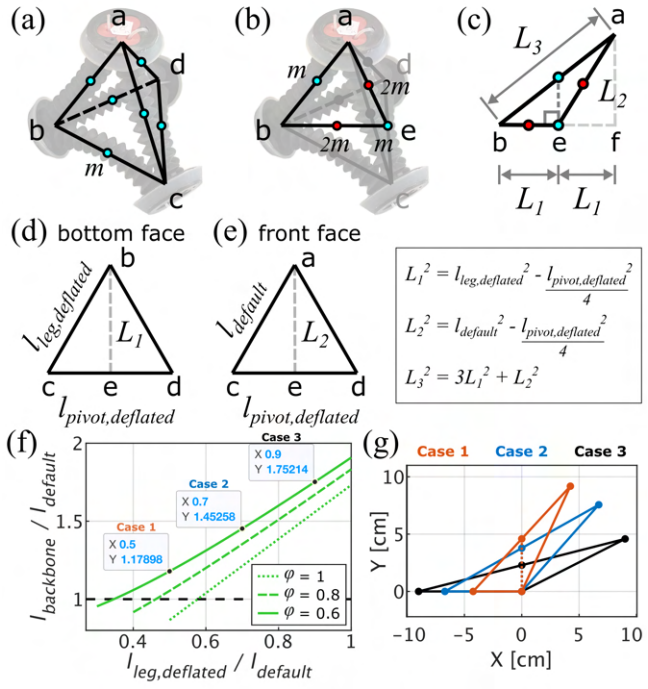

Fig. 3: Geometry diagram for rolling from face A to B. (a) Isometric view of Tetraflex, presenting a bellow as a line with a point mass m at the line centre. (b-c) Triangular cross sections at (b) a default shape and (c) a deformed shape just before rolling. Green and red dots define point mass of m and $2m$ (representing two bellows), respectively. (d) Bottom face and (e) front face of Tetraflex. Inset box shows relationship equations of triangular lines L_1, L_2 and L_3. (f) Relationship between deflated lengths of leg bellows and length of the backbone bellow to achieve rolling, where $\varphi = l_{pivot,deflated}/l_{default}$. (g) Examples of Tetraflex at different rolling conditions: $l_{leg,deflated}/l_{default}$ at 0.5, 0.7 and 0.9 while φ = 0.6, as Case 1, 2 and 3, as stated in (f).

IEEE Robotics and Automation Letters (RA-L) paper, presented at ICRA 2024, Yokohama, Japan. Cite as RA-L paper.

IEEE Robotics and Automation Letters (RA-L) paper, presented at ICRA 2024, Yokohama, Japan. Cite as RA-L paper.

centre of the pivot bellow bellow, point e, and projecting the other out-of-plane bellows as point masses onto this triangle abe (Fig. 3b). We define L_1, L_2 and L_3 as the side lengths of this projected triangle.

To derive the rolling condition we consider the point at which Tetraflex is on the verge of toppling over, where the COM of the robot is above the pivot point e (Fig. 3c). To perform rolling, the leg bellows ($\overline{bc}$ and $\overline{bd}$) and the pivot bellow ($\overline{cd}$) are contracted to the length $l_{leg,deflated}$ and $l_{pivot,deflated}$, respectively, and the backbone below ($\overline{ab}$) is extended to length $l_{backbone}$. The other two bellows remain at $l_{default}$. By considering the geometry of Tetraflex under this state and referring to Fig. 3c-e, the relationship between these lengths is derived as an equation below.

$$\left(\frac{l_{backbone}}{l_{default}}\right)^2 = 3\cdot\left(\frac{l_{leg,deflated}}{l_{default}}\right)^2 + \left(1-\left(\frac{l_{pivot,deflated}}{l_{default}}\right)^2\right)$$

Note that the minimum $l_{leg,deflated}$ must be higher than half of $l_{pivot,deflated}$, referred to Fig. 3d. Hence, the relationship between $l_{leg,deflated}$ and $l_{backbone}$ to achieve rolling is illustrated in Fig. 3f, where φ is the ratio of $l_{pivot,deflated}$ to $l_{default}$. It can be concluded that larger deflation of the leg bellows (shorter $l_{leg,deflated}$) requires less inflation of the backbone bellow (shorter $l_{backbone}$). Alternatively, rolling can occur by only deflating the leg bellows to $l_{leg,deflated}$ where $l_{backbone}/l_{default} \leq 1$ or by inflation of the backbone bellow to $l_{backbone}$ where $l_{leg,deflated}/l_{default} = 1$ (Fig. 3f). Moreover, in reality the pivot bellow buckles outwards in leg bellow contraction, impeding the roll. Hence, deflating pivot bellow (or decreasing φ) facilitates easier rolling. Rolling examples when constraining $l_{pivot,deflated}$ at $\varphi = 0.6$ for different $l_{leg,deflated}/l_{default}$ at 0.5, 0.7 and 0.9 (Case 1, 2 and 3 from Fig. 3f, respectively) are shown in Fig. 3g.

2) Crawling: The crawling locomotion utilises a stick and slip mechanism. To explain the mechanism, we consider locomotion with the ground face A and the movement direction towards face D. Both structural bellows are initially deflated then held at the minimum bellow length for the duration of the crawling (Fig. 5b). The remaining four bellows form two groups dependant on their positions. 'Under' bellows lie on the ground face ($\overline{bd}$, $\overline{cd}$) and 'over' bellows on the front face ($\overline{ab}$, $\overline{ac}$) as shown in (Fig. 4).

A crawling cycle consists of 4 consecutive stages: under group contraction; over group contraction; under group extension; and over group extension (Fig. 5b).

In stage 1, the 'under' bellows group contracts. The contact angle at the rear node changes during this motion so that the (low friction) exposed PLA of the end cap contacts the surface, allowing it to slide forwards and under the robot. In stage 2 the upper bellows group also contracts, reducing the length of Tetraflex. In stage 3 the under group is inflated, then in stage 4 the over group is inflated, pushing the front of Tetraflex forwards. The rear node of Tetraflex changes pitch through stage 3, bringing the high friction elastomer section of the end cap in contact with the surface. At the same time, the front end of Tetraflex is relatively unweighted allowing it to be pushed forwards as the bellows expand.

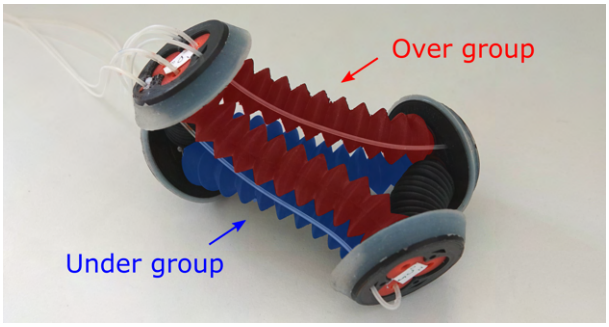

Fig. 4: The extended phase of the crawling/bounding locomotion (stage 4), with the under group and over group highlighted in blue and red respectively.

3) Bounding: If we increase the contraction of the under group in the crawling sequence by applying the negative pressure for a longer duration, we generate a bounding gait (Fig. 5c). Applying the crawling control sequence, but increasing the contraction of the under bellows causes a more exaggerated rearward shift of the COM in the contractile stages, causing Tetraflex to roll backwards onto the rear node and the front end to lift off the ground. Subsequent inflation of the under group bellows pushes the lifted front end forward, taking a large step.

III. Results

As for the effectiveness of Tetraflex's locomotion strategies, we characterise their velocity and consistency over a number of consecutive cycles. Velocity is calculated by dividing the displacement by time taken. This is different from on-board/intrinsic speed for the rolling gait as it takes a zig-zag path rather than travelling in a straight line. The consistency of the gaits has two components: rotational deviation and linear deviation per displacement. Rotational deviation is how much Tetraflex spins around its own axis, resulting in a misalignment between Tetraflex's heading and its odometry. Linear deviation per displacement is the distance between the robot's end location and the mean end location, averaged over all 5 trials. This value is normalised by the net distance covered in order to compare the different gaits. A zero value would mean that the robot finished in precisely the same location over all trials. The pressures used during these tests are presented in Table I.

TABLE I: Pressures used in different gaits (kPa)

Applied pressure	Rolling atm	Rolling 17 kPa	Rolling 35 kPa	Crawling	bounding
P_{high}	80	80	80	80	80
P_{low}	atm	17	35	atm	atm
P_{-ve}	-20	-20	-20	-20	-20

A. Size Change

Individual bellows were able to smoothly expand from their natural length (106.3±1.6 mm at atm) with positive increasing pressure, extending to 147.1±3.1 mm (138% natural length) at an applied pressure of 75 kPa (Fig. 6). Under negative pressure, the bellows contracted. The pressure at which a

IEEE Robotics and Automation Letters (RA-L) paper, presented at ICRA 2024, Yokohama, Japan. Cite as RA-L paper.

IEEE Robotics and Automation Letters (RA-L) paper, presented at ICRA 2024, Yokohama, Japan. Cite as RA-L paper.

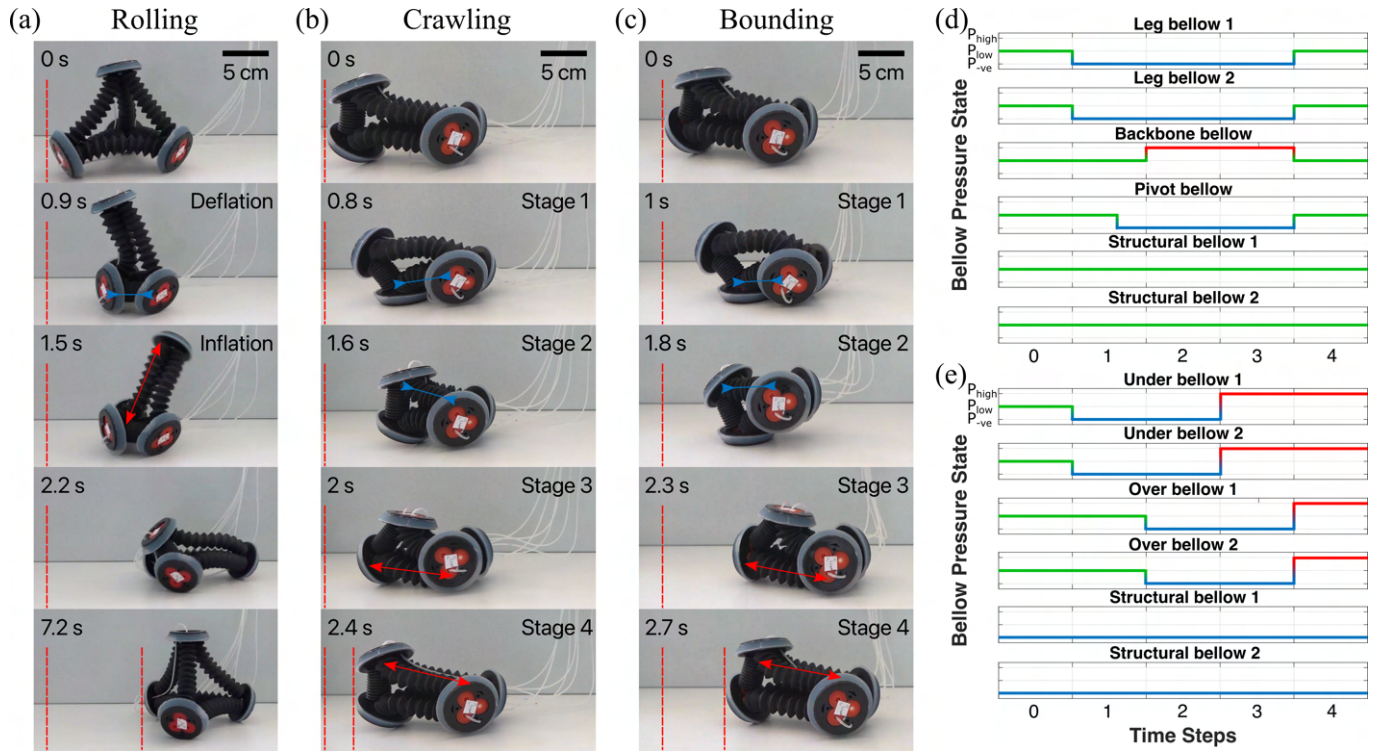

Fig. 5: (a-c) Sequential images of Tetraflex rolling, crawling and bounding. Arrows depict bellow actuation (blue arrow = contraction, red arrow = elongation). Sequences of bellow actuation in one cycle are as follows. (a) Rolling: the 'leg bellows' and the pivot (hidden in the figure) contract, then the 'backbone' bellow extends. (b) Crawling: Under group followed by the over group contract, then extend. (c) Bounding: Same sequence as crawling, but with more contraction of the 'under' bellows'. (d-e) Control sequence showing applied pressures for (d) rolling and (e) crawling/bounding. Stage 1 of bounding is longer than that of crawling, the extra time means that the frontal bellow lifts off the ground in Stage 2 of bounding. Green represents default pressure P_{low} (atm, 17 kPa or 35 kPa), blue for the contraction P_{-ve} (-20 kPa) pressure and red for the expansion pressure P_{high} (80 kPa).

bellow fold collapsed during contraction ranged from -5 to -15 kPa. This variance is due to slight differences in material thickness coupled with the intrinsic instability that is present as bellow folds collapse. All bellows reached their fully contracted length of 44.6±0.25 mm (42% natural length) at pressures below -20 kPa. To evaluate the rolling performance of Tetraflex at different default sizes, three positive pressures were chosen within the working range of the bellows (Fig. 1a). The respective bellow lengths and estimated robot volume at each pressure are: 106.3±1.6 mm and 141 cm^3 at atm, 120.2±1.2 mm and 205 cm^3 at 17 kPa, 130.0±1.3 mm and 259 cm^3 at 35 kPa, and 44.6±0.25 mm and 10.5 cm^3 when fully contracted. For atm the bellows bend inwards to a maximum deflection of 8.51±0.3 mm, for 17 kPa maximum deflection was 11.04±0.3 mm and for 35 kPa the maximum deflection was 11.39±0.4 mm.

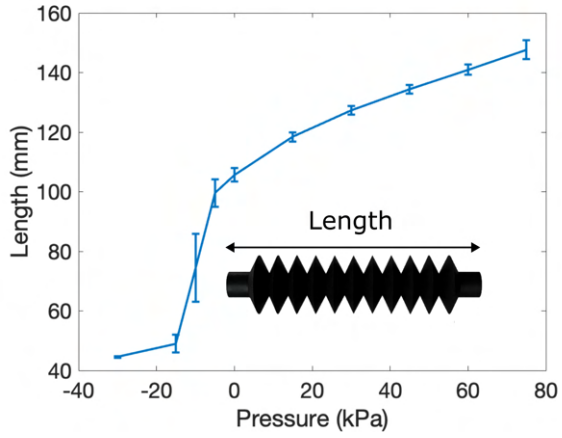

Fig. 6: Relationship between length and pressure of four individual bellow actuators. Error bar presents one standard deviation.

B. Locomotion Results

1) Rolling: Accurate odometry relies on consistent and predictable behaviour. Hence we assessed the consistency and speed of the rolling gait over four rolls with three different default sizes (corresponding to different P_{low} inputs of atm, 17 kPa and 35 kPa), by performing five trials of four rolling cycles. Fig. 7a-c visualizes these trials. Showing the initial position, the five end poses and a mean end pose, we assess the consistency of these trials by comparing the spread of trials relative to the mean end pose.

IEEE Robotics and Automation Letters (RA-L) paper, presented at ICRA 2024, Yokohama, Japan. Cite as RA-L paper.

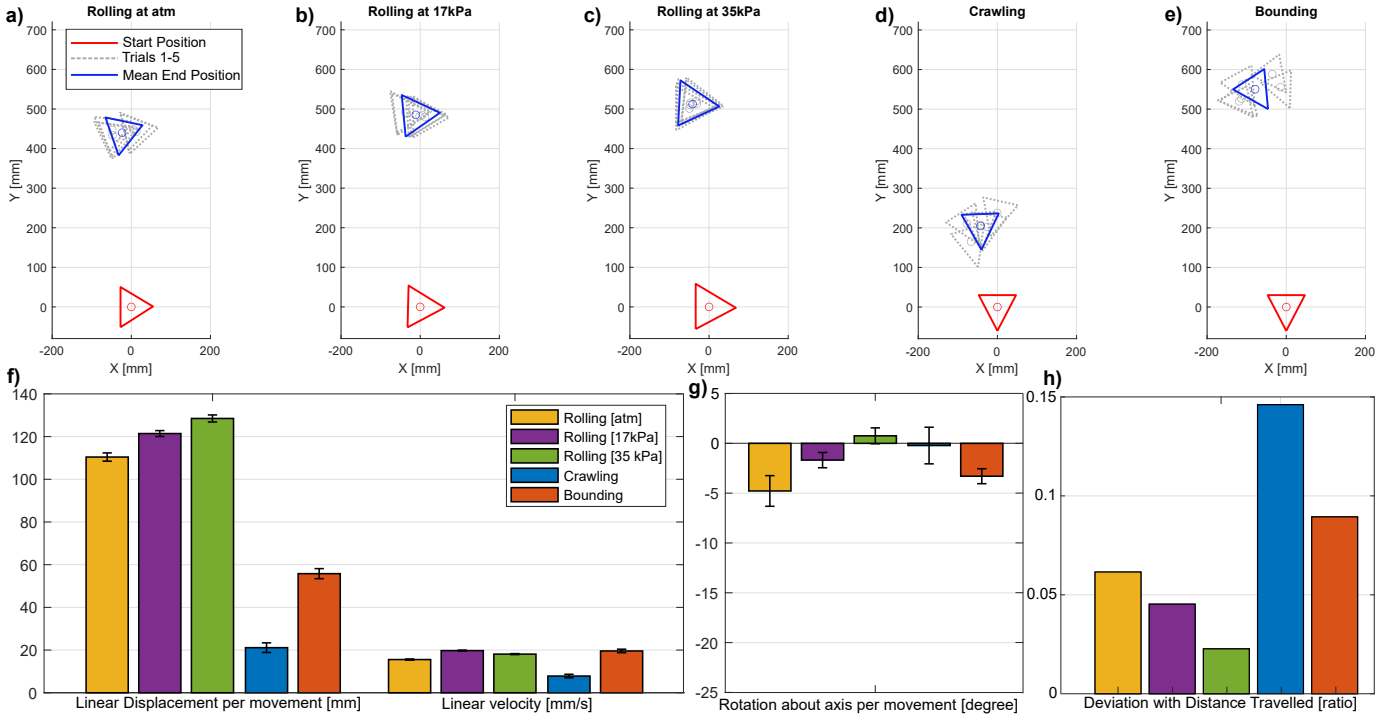

Fig. 7: (a-e) Plot of movement, location and orientation of Tetraflex after four (rolling) movements or ten (crawling, bounding). Rolling performed at three default pressures (c-e). (f) Comparison of the linear displacement and velocity of each mode; error bar indicates standard deviation calculated over 5 trials. (g-h) Comparison of (g) angular deviation and (h) distance deviation of each mode.

The mean distance per roll increased as Tetraflex's default pressure, and therefore size, was increased (110.4±1.73 mm, 121.4±1.24 mm and 128.50±1.47 mm at atm, 17 kPa, and 35 kPa respectively, Fig. 7f). The linear velocity does not follow the same relationship (15.6±0.27 mm/s, 19.7±0.22 mm/s and 18.10±0.23 mm/s at atm, 17 kPa, and 35 kPa respectively, Fig. 7f) because longer inflation times were required to attain the higher pressures, resulting in slower steps. The 17 kPa default size was the fastest, followed by 35 kPa and finally atm (Fig. 7f). This demonstrates that the benefit of a larger step size is not always worth the cost of a longer inflation time when optimizing for speed.

Both the angular deviation per movement and linear deviation per displacement (Fig. 7g and Fig. 7h) reduce as the default size of Tetraflex increases. This indicates more accurate odometry for larger sizes of Tetraflex. The deviation from the target position after four movements remained small, suggesting that the odometry can accurately predict robot position relative to a start point using just the control inputs. Based on the results, we plotted a tessellation map to visualize the motion of Tetraflex rolling at different sizes (Fig. 8). This map can be used to help understand reacheable positions of Tetraflex by rolling and do motion planning.

2) Crawling and bounding: Tetraflex performed five trials for both crawling and bounding gaits, each comprising of ten movement cycles (Fig. 7a-b). By varying a single control parameter (deflation time), Tetraflex changes between these two distinct gaits (Fig. 5b-c). The crawling locomotion utilises a friction asymmetry between the front and back to achieve

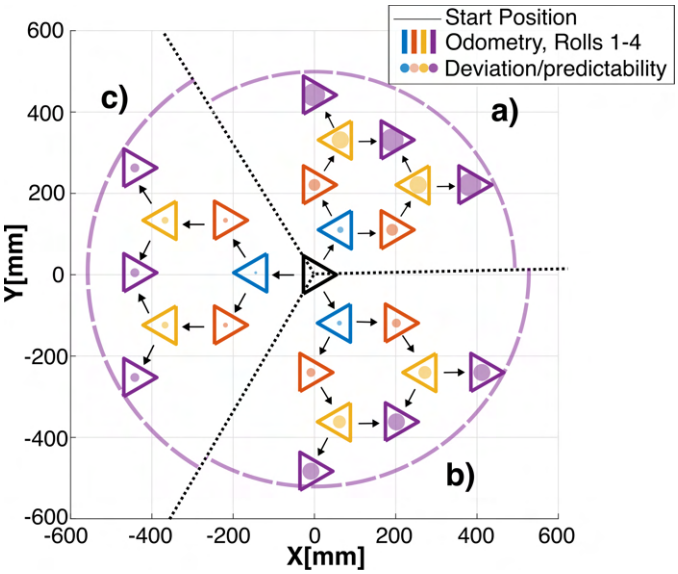

Fig. 8: Tessellation map showing the motion of Tetraflex when rolling at different default sizes. The map is split into 3 sections: a) atmospheric pressure, b) 17 kPa, c) 35 kPa. The dashed purple line shows the maximum distance travelled from the centre-point for each pressure after 4 rolls. A circle whose radius equals the expected deviation (calculated over 5 trials) in position is plotted in the middle of the each position projection.

IEEE Robotics and Automation Letters (RA-L) paper, presented at ICRA 2024, Yokohama, Japan. Cite as RA-L paper.

IEEE Robotics and Automation Letters (RA-L) paper, presented at ICRA 2024, Yokohama, Japan. Cite as RA-L paper.

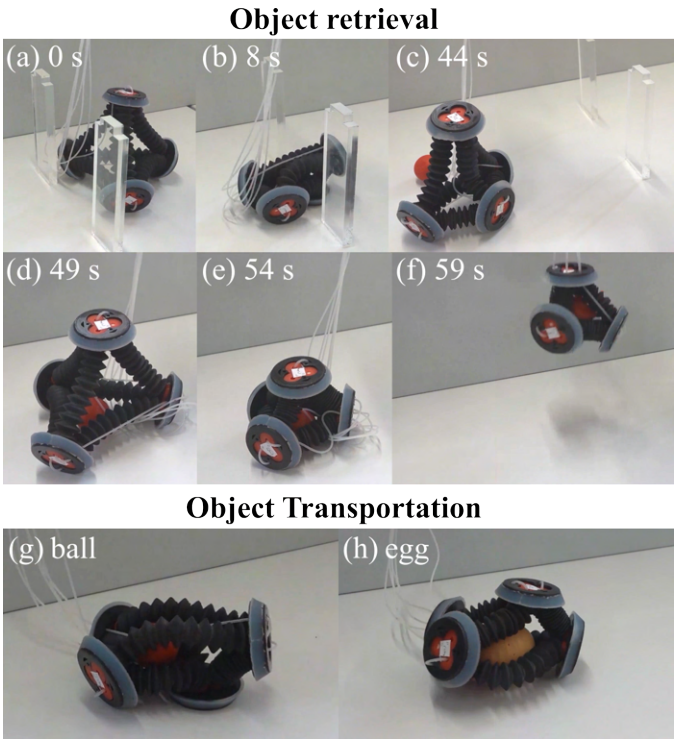

Fig. 9: Demonstration of Tetraflex retrieving and transporting objects. (a-f) Tetraflex retreving; (a) Tetraflex at default size, (b) bounding through a narrow gap, (c) rolling to, (d) rolling over, (e) engulfing a target object, i.e., a red ball, and (f) retrieving Tetraflex. Alternatively, after engulfing the object, Tetraflex can crawl with it for transportation: (g) the red ball or (h) the egg. (see Supplementary movie S1).

small steps, whilst increasing the lower group contraction causes the Tetraflex to lift its front off the ground and take larger steps in a bounding locomotion (Fig. 7f). The bounding locomotion achieves the highest speed of all locomotion types (19.6±0.83 mm/s), whilst the crawling gait achieves the lowest speed (7.82±0.83 mm/s). The large frictional interaction between Tetraflex and the substrate in these modes means that their odometry is less predictable than for the rolling gaits (Fig. 5h).

C. Object Retrieval Demonstration

Tetraflex can combine its multi-gait versatility with the capability to engulf and carry objects, and thereby demonstrate effective object retrieval. Here Tetraflex uses bounding locomotion to pass through a narrow gap (width = 80 mm, equal to 0.625 of default robot width at atm pressure), then roll to a target object. Tetraflex then expands as required by the object size and rolls over the object, contracting the bellows to engulf it. Finally, Tetraflex uses crawling locomotion to transport the object whilst providing protection from the environment (Fig. 9 and Supplementary video S1).

IV. Discussion

Tetraflex has demonstrated the potential for the Polyflex concept to generate large morphological adaptability in simple and scalable soft robots. The three gaits of rolling, crawling and bounding were investigated. By coordinating bellows pressures, additional capabilities of passing through small gaps and picking up and transporting objects were demonstrated. The maximum locomotion speed can be achieved by bounding (19.6 mm/s, 0.15 BL/s), with rolling showing a range of lower speeds, depending on bellows pressure (15.6 - 19.4 mm/s, 0.12 - 0.15 BL/s) and crawling the slowest (7.82 mm/s, 0.06 BL/s). Note that the body length per second values are based upon a Tetraflex of size corresponding to atm pressure, with a body length of 128 mm (this value includes the extra size due to the end caps). Tetraflex rolling results with increased default sizes give an overestimated BL/s relative to the size of the robot when the experiment was carried out. Rolling locomotion was found to be best for accurate odometry, with the 35 kPa default size showing less than 3% deviation per distance travelled. The other rolling default sizes produced less accurate rolls. Considering smaller sizes of Tetraflex (corresponding to atm and 17 kPa pressures), when rolling the ratio of extended bellow length to default bellow length is greater, moving the centre of mass further outside the base of support and creating a greater rolling moment, we expect this leads to higher slip on landing. Fig. 8 shows a top down view of the movement pattern of Tetraflex, which moves on a triangular grid. The central triangle represents the starting position of Tetraflex and the coloured triangles represent Tetraflex position after 1, 2, 3 and 4 rolls. The central circle within the triangles has a radius which corresponds with the expected linear deviation (shown in Fig. 7). The default size, and thus the resolution of the grid can be varied on the fly to achieve closer positioning to the target location, see Fig. 8 a-c which demonstrate the change in step size for different default sizes of Tetraflex.

When finer movement resolution is required, the bounding and crawling gaits can be used to make smaller steps with their medium (55.8 mm) and small (21.1 mm) step sizes respectively (compared to 110-129 mm for rolling). These gaits also have the benefit of reducing the height and width of Tetraflex from 128 mm to 80 mm, allowing passage through narrow gaps that are inaccessible to a default size Tetraflex (Fig. 9). However, they have the highest linear deviation per distance travelled making them less suited to odometry.

By combining the strengths of its different gaits, we can plan Tetraflex's route to some arbitrary point by discretising the space into a triangular tessellation grid of the desired resolution, then roll to the grid point closest to the target location. If necessary it can then crawl or bound for fine adjustment of position, or to pass through a narrow gap to reach an objective. No issues with air tube entanglement were identified in the tests. Future work will explore the integration of soft and flexible on-board pneumatic compression [32], [33] to untether Tetraflex from the supply tubing. The shape and size change capabilities of Tetraflex bring great versatility and adaptability. One benefit of the soft open truss architecture is transport of objects within the robot itself (see Fig. 9). This has potential for sample retrieval in challenging environments, and handling fragile or biological objects because the soft truss structure protects the payload. We demonstrate how Tetraflex can roll onto objects as large as an egg and grasp/engulf

them. Once an object is engulfed, the robot's movements are constrained to prevent release of the object. In this state, Tetraflex is still able to locomote with the payload using the crawling gait. A thorough exploration of these constraints and Tetraflex's ability to operate within them will be a future investigation, whereas the current study demonstrates its feasibility. Additionally, further investigation should include a wider study to characterise the larger Polyflex family by changing number of struts (e.g., 12 struts for cubeflex) and adapting the design of the end caps to accommodate different number of struts.

Tetraflex demonstrates the potential of the Polyflex architecture and shows how a simple, adaptable, flexible and modular soft robot can locomote to, grasp/engulf and then transport objects. The consistency and speed of rolling, crawling and bounding gaits are evaluated. We also show that Tetraflex can utilise the rolling gait to locomote accurately on a discretised grid, with the crawling and bounding gaits being used for smaller steps. Finally we show Tetraflex rolling onto and engulfing a fragile object before carrying it, safely held within the robot. Future work will explore higher level locomotion planning algorithms and theoretical analysis. Gait transitions and full autonomous and untethered operations will also be explored. A particular focus for autonomy will be to integrate soft sensors into the centre axis or the shells of the bellow actuators. Modelling and simulation of Tetraflex gaits, and comparison of those gaits to robots of similar structures in accuracy and other measures, will also be the subject of future study. Tetraflex, and the generalised Polyflex architecture, enable a new family of soft, morphologically adaptable soft robot for a wide range of applications including environmental exploration and search and rescue.

REFERENCES

[1] R. E. Skelton and M. C. De Oliveira, *Tensegrity systems*. Springer, 2009, vol. 1.

[2] D. S. Shah, J. W. Booth, R. L. Baines, K. Wang, M. Vespignani, K. Bekris, and R. Kramer-Bottiglio, "Tensegrity robotics," *Soft robotics*, vol. 9, no. 4, pp. 639–656, 2022.

[3] M. Vespignani, J. M. Friesen, V. SunSpiral, and J. Bruce, "Design of superball v2, a compliant tensegrity robot for absorbing large impacts," in *2018 IEEE/RSJ International Conference on Intelligent Robots and Systems (IROS)*. IEEE, 2018, pp. 2865–2871.

[4] G. J. Hamlin and A. C. Sanderson, "Tetrobot: A modular approach to parallel robotics," *IEEE Robotics & Automation Magazine*, vol. 4, no. 1, pp. 42–50, 1997.

[5] S. Curtis, M. Brandt, G. Bowers, G. Brown, C. Cheung, C. Cooperider, M. Desch, N. Desch, J. Dorband, K. Gregory *et al.*, "Tetrahedral robotics for space exploration," in *2007 IEEE Aerospace Conference*. IEEE, 2007, pp. 1–9.

[6] W. H. Lee and A. C. Sanderson, "Dynamic analysis and distributed control of the tetrobot modular reconfigurable robotic system," *Autonomous Robots*, vol. 10, no. 1, pp. 67–82, 2001.

[7] K. Cook and M. Abrahantes, "Gait design for a tetrahedral worm," in *2016 IEEE International Conference on Electro Information Technology (EIT)*. IEEE, 2016, pp. 0621–0626.

[8] M. Abrahantes, L. Nelson, and P. Doorn, "Modeling and gait design of a 6-tetrahedron walker robot," in *2010 42nd Southeastern Symposium on System Theory (SSST)*. IEEE, 2010, pp. 248–252.

[9] M. Abrahantes and C. Smits, "Implementation and control of a reconfigurable 8-tetrahedral robot," in *2012 IEEE International Conference on Electro/Information Technology*. IEEE, 2012, pp. 1–5.

[10] Y. Tian and Y.-A. Yao, "Dynamic rolling analysis of triangular-bipyramid robot," *Robotica*, vol. 33, no. 4, pp. 884–897, 2015.

[11] J. Gu, Y. Lin, Q. Cui, X. Li, J. Li, L. Sun, C. Yao, F. Ying, G. Wang, and L. Yao, "Pneumesh: Pneumatic-driven truss-based shape changing system," in *Proceedings of the 2022 CHI Conference on Human Factors in Computing Systems*, 2022, pp. 1–12.

[12] N. S. Usevitch, Z. M. Hammond, M. Schwager, A. M. Okamura, E. W. Hawkes, and S. Follmer, "An untethered isoperimetric soft robot," *Science Robotics*, vol. 5, no. 40, p. eaaz0492, 2020.

[13] Y. Masuda and M. Ishikawa, "Development of a deformation-driven rolling robot with a soft outer shell," in *2017 IEEE International Conference on Advanced Intelligent Mechatronics (AIM)*. IEEE, 2017, pp. 1651–1656.

[14] H.-T. Lin, G. G. Leisk, and B. Trimmer, "Goqbot: a caterpillar-inspired soft-bodied rolling robot," *Bioinspiration & biomimetics*, vol. 6, no. 2, p. 026007, 2011.

[15] J. Wang, Y. Fei, and Z. Liu, "Locomotion modeling of a triangular closed-chain soft rolling robot," *Mechatronics*, vol. 57, pp. 150–163, 2019.

[16] A. Yin, H.-C. Lin, J. Thelen, B. Mahner, and T. Ranzani, "Combining locomotion and grasping functionalities in soft robots," *Advanced Intelligent Systems*, vol. 1, no. 8, p. 1900089, 2019.

[17] L. Xu, R. J. Wagner, S. Liu, Q. He, T. Li, W. Pan, Y. Feng, H. Feng, Q. Meng, X. Zou *et al.*, "Locomotion of an untethered, worm-inspired soft robot driven by a shape-memory alloy skeleton," *Scientific reports*, vol. 12, no. 1, pp. 1–16, 2022.

[18] G. Mao, D. Schiller, D. Danninger, B. Hailegnaw, F. Hartmann, T. Stockinger, M. Drack, N. Arnold, and M. Kaltenbrunner, "Ultra-fast small-scale soft electromagnetic robots," *Nature communications*, vol. 13, no. 1, pp. 1–11, 2022.

[19] Y.-B. Tian and Y.-A. Yao, "Constructing rolling mechanisms based on tetrahedron units," in *Advances in Reconfigurable Mechanisms and Robots I*. Springer, 2012, pp. 221–232.

[20] S. Park, E. Park, M. Yim, J. Kim, and T. W. Seo, "Optimization-based nonimpact rolling locomotion of a variable geometry truss," *IEEE Robotics and Automation Letters*, vol. 4, no. 2, pp. 747–752, 2019.

[21] F. Zhang, Y. Yu, Q. Wang, and X. Zeng, "Physics-driven locomotion planning method for a planar closed-loop terrain-adaptive robot," *Mechanism and Machine Theory*, vol. 162, p. 104353, 2021.

[22] G. M. Whitesides, "Soft robotics," *Angewandte Chemie International Edition*, vol. 57, no. 16, pp. 4258–4273, 2018.

[23] S. Kim, C. Laschi, and B. Trimmer, "Soft robotics: a bioinspired evolution in robotics," *Trends in biotechnology*, vol. 31, no. 5, pp. 287–294, 2013.

[24] L. Zhang, S. Bi, and Y. Cai, "Design and motion analysis of tetrahedral rolling robot," in *2010 IEEE/RSJ International Conference on Intelligent Robots and Systems*. IEEE, 2010, pp. 502–507.

[25] Z. Wang, Y. Li, B. Su, L. Jiang, Z. Zhao, and Y.-A. Yao, "Design and locomotion analysis of the tetrahedral mobile robot with only revolute joints (tmrr)," *Industrial Robot: the international journal of robotics research and application*, 2021.

[26] R. Liu, Y.-a. Yao, and Y. Li, "Design and analysis of a deployable tetrahedron-based mobile robot constructed by sarrus linkages," *Mechanism and Machine Theory*, vol. 152, p. 103964, 2020.

[27] Y. Li, Z. Wang, Y. Xu, J. S. Dai, Z. Zhao, and Y.-a. Yao, "A deformable tetrahedron rolling mechanism (dtrm) based on uru branch," *Mechanism and Machine Theory*, vol. 153, p. 104000, 2020.

[28] J. A. Rivera and C. J. Kim, "Spatial parallel soft robotic architectures," in *2014 IEEE/RSJ International Conference on Intelligent Robots and Systems*. IEEE, 2014, pp. 548–553.

[29] W.-H. Tian, C.-C. Jhan, M. Inokuma, T. Akagi, S. Dohta, and S. Shimooka, "Development of a tetrahedral-shaped soft robot arm as a wrist rehabilitation device using extension type flexible pneumatic actuators," *Journal of Robotics and Mechatronics*, vol. 32, no. 5, pp. 931–938, 2020.

[30] N. S. Usevitch, A. M. Okamura, and E. W. Hawkes, "Apam: antagonistic pneumatic artificial muscle," in *2018 IEEE International Conference on Robotics and Automation (ICRA)*. IEEE, 2018, pp. 1539–1546.

[31] Y. Wang, J. Wang, and Y. Fei, "Design and modeling of tetrahedral soft-legged robot for multi-gait locomotion," *IEEE/ASME Transactions on Mechatronics*, 2021.

[32] C. Cao, X. Gao, and A. T. Conn, "A magnetically coupled dielectric elastomer pump for soft robotics," *Advanced Materials Technologies*, vol. 4, no. 8, p. 1900128, 2019.

[33] R. S. Diteesawat, T. Helps, M. Taghavi, and J. Rossiter, "Electro-pneumatic pumps for soft robotics," *Science robotics*, vol. 6, no. 51, p. eabc3721, 2021.

IEEE Robotics and Automation Letters (RA-L) paper, presented at ICRA 2024, Yokohama, Japan. Cite as RA-L paper.